

UNIVERSIDADE ESTADUAL DE CAMPINAS
SISTEMA DE BIBLIOTECAS DA UNICAMP
REPOSITÓRIO DA PRODUÇÃO CIENTÍFICA E INTELLECTUAL DA UNICAMP

Versão do arquivo anexado / Version of attached file:

Versão do Editor / Published Version

Mais informações no site da editora / Further information on publisher's website:

<https://www.mdpi.com/2073-4409/12/19/2418>

DOI: <https://doi.org/10.3390/cells12192418>

Direitos autorais / Publisher's copyright statement:

©2023 by MDPI. All rights reserved.

DIRETORIA DE TRATAMENTO DA INFORMAÇÃO

Cidade Universitária Zeferino Vaz Barão Geraldo



CEP 13083-970 – Campinas SP

Fone: (19) 3521-6493

<http://www.repositorio.unicamp.br>

Article

Mapping Cell-in-Cell Structures in Oral Squamous Cell Carcinoma

Leonardo de Oliveira Siquara da Rocha ^{1,2}, Bruno Solano de Freitas Souza ^{1,3}, Ricardo Della Coletta ^{4,5} , Daniel W. Lambert ⁶  and Clarissa A. Gurgel Rocha ^{1,2,3,7,*} 

¹ Gonçalo Moniz Institute, Oswaldo Cruz Foundation (IGM-FIOCRUZ/BA), Salvador 40296-710, BA, Brazil; leonardo.oliveira@ufba.br (L.d.O.S.d.R.); bruno.solano@fiocruz.br (B.S.d.F.S.)

² Department of Pathology and Forensic Medicine, School of Medicine, Federal University of Bahia, Salvador 40110-100, BA, Brazil

³ D'Or Institute for Research and Education (IDOR), Salvador 41253-190, BA, Brazil

⁴ Department of Oral Diagnosis, School of Dentistry, University of Campinas, Piracicaba 13414-903, SP, Brazil

⁵ Graduate Program in Oral Biology, School of Dentistry, University of Campinas, Piracicaba 13414-903, SP, Brazil

⁶ School of Clinical Dentistry, The University of Sheffield, Sheffield S10 2TA, UK

⁷ Department of Propaedeutics, School of Dentistry, Federal University of Bahia, Salvador 40110-150, BA, Brazil

* Correspondence: clarissa.gurgel@fiocruz.br or gurgel.clarissa@gmail.com;

Tel.: +55-71-3176-2209 or +55-71-3176-2289

Abstract: Cell-in-cell (CIC) structures contribute to tumor aggressiveness and poor prognosis in oral squamous cell carcinoma (OSCC). In vitro 3D models may contribute to the understanding of the underlying molecular mechanisms of these events. We employed a spheroid model to study the CIC structures in OSCC. Spheroids were obtained from OSCC (HSC3) and cancer-associated fibroblast (CAF) lines using the Nanoshuttle-PL™ bioprinting system (Greiner Bio-One). Spheroid form, size, and reproducibility were evaluated over time (Evos™ XL; ImageJ version 1.8). Slides were assembled, stained (hematoxylin and eosin), and scanned (Axio Imager Z2/VSLIDE) using the OlyVIA System (Olympus Life Science) and ImageJ software (NIH) for cellular morphology and tumor zone formation (hypoxia and/or proliferative zones) analysis. CIC occurrence, complexity, and morphology were assessed considering the spheroid regions. Well-formed spheroids were observed within 6 h of incubation, showing the morphological aspects of the tumor microenvironment, such as hypoxic (core) and proliferative zone (periphery) formation. CIC structures were found in both homotypic and heterotypic groups, predominantly in the proliferative zone of the mixed HSC3/CAF spheroids. “Complex cannibalism” events were also noted. These results showcase the potential of this model in further studies on CIC morphology, formation, and relationship with tumor prognosis.

Keywords: tumor spheroids; oral squamous cell carcinoma; cell cannibalism; cell-in-cell structures; cancer-associated fibroblasts



Citation: Siquara da Rocha, L.d.O.; Souza, B.S.d.F.; Coletta, R.D.; Lambert, D.W.; Gurgel Rocha, C.A. Mapping Cell-in-Cell Structures in Oral Squamous Cell Carcinoma. *Cells* **2023**, *12*, 2418. <https://doi.org/10.3390/cells12192418>

Academic Editor: Ritva Tikkanen

Received: 27 July 2023

Revised: 10 September 2023

Accepted: 11 September 2023

Published: 8 October 2023



Copyright: © 2023 by the authors. Licensee MDPI, Basel, Switzerland. This article is an open access article distributed under the terms and conditions of the Creative Commons Attribution (CC BY) license (<https://creativecommons.org/licenses/by/4.0/>).

1. Introduction

Over 350,000 new oral cancer cases are diagnosed yearly worldwide [1]. Oral squamous cell carcinoma (OSCC) represents over 90% of these [2–4], with a mortality rate of over 60% in five years [5,6]. The aggressive treatment regimens frequently required have severe impacts on the quality of life of survivors. Advances in the knowledge of OSCC pathogenesis, diagnostics, and therapeutics are hampered by the limited in vitro reproduction of the complex characteristics of tumor biology [7–9].

Among the events that take place in tumors, the occurrence of cell-in-cell (CIC) structures has drawn increasing attention because of their relationship with poorer prognosis in cancers such as lung cancer [10], breast cancer [11], and OSCC [12,13]. Classically known as “signet ring” or “bird’s eye” cells, these events are commonly defined as morphological findings of one cell within another [14–17], resulting from the distinct mechanisms of

non-professional engulfment of living cells by their pairs [18]. Studies investigating the presence of CIC structures suggest that their incidence is a tumoral response to hostile circumstances, such as starvation [19,20], hypoxia [21], or chemo- and radiotherapy [11,22]. This mechanism enhances cell survival [23], immune escape [24], treatment resistance [25], and the selection of an aggressive cell population [26,27].

In addition, the tumor microenvironment (TME), composed mainly of non-tumoral cells, extracellular matrix, and blood vessels that support the tumor [28,29], also plays an essential role in tumor aggressiveness [30]. Cancer-associated fibroblasts (CAF), for example, interact with the tumor and the extracellular matrix, changing tumor metabolism [31,32] and motility [33], contributing to tumor invasion [34], resistance [35,36], and metastasis [37,38].

Commonly used two-dimensional cell culture models do not adequately reproduce many features of the tumor microenvironment, such as zone formation (e.g., quiescent and proliferative zones), oxygen and nutrient gradients, and complex cellular interactions [39,40]. Alternatively, preclinical research relies on animal models, such as mice or rats, which can characterize tumor pathogenesis [41]. Nevertheless, these methods have limitations, such as the inadequate reproduction of the systemic anti-tumoral immune response in immunodeficient animals used for tumor xenografts [41,42]. In this context, three-dimensional models aim to bridge the gap between *in vitro* cultures and *in vivo* tumors [29,43], simulating, for example, hypoxia and metabolic changes in the tumor microenvironment [44–46]. These models have been applied to study cancer complexities in the breast [47,48], kidney [49] carcinomas, neuroblastoma [50], and OSCC [51], for example.

Given the evidence of the contribution of CIC structures to the aggressiveness of OSCC, here we aimed to detail morphological aspects of these events, considering homotypic and heterotypic (CAF) cellular interactions and the formation of tumor zones, by employing a 3D bioprinting *in vitro* model to study these structures for the first time.

2. Materials and Methods

2.1. Cell Culture

The cell lines used in this study were a metastatic OSCC line obtained from the tongue (HSC3—JCRB, Osaka, Japan) and a primary cancer-associated fibroblast isolated from tongue OSCC (CAF1 [52], ethics committee approval number 4,706,681). Tumor cells were cultured in DMEM High-Glucose medium (Gibco™, Waltham, MA, USA), supplemented with 10% fetal bovine serum (FBS—Gibco™, Waltham, MA, USA) and 0.8% hydrocortisone (Sigma-Aldrich™, Gillingham, UK). Fibroblasts were cultured in DMEM/F-12 medium (Gibco™, Waltham, MA, USA), supplemented with 10% newborn calf serum (CALF—Gibco™, Waltham, MA, USA). Both cultures were supplemented with 1% antibiotics (Pen Strep, Gibco™, Waltham, MA, USA) and assessed for mycoplasma monthly. Cells were kept in incubators at 5% CO₂ and 37 °C. A total of 70–80% of cell confluence was set for trypsinization (trypsin 0.5% 10×, Gibco™, Waltham, MA, USA). CAFs were cultured up to the 10th passage.

2.2. Spheroid Formation

Tumor spheroids were obtained using the magnetic bioprinting Bio-Assembler™ System (Greiner Bio-One, Kremsmünster, Austria). Briefly, this method relies on cellular membrane magnetization using biocompatible nanoparticles (Nanoshuttle-PL™, Greiner Bio-One, Kremsmünster, Austria) composed of gold, iron oxide, and poly-L-lysine. Magnetic nanoparticles measured approximately 50 nm in diameter [53] and adhered electrostatically to the cellular membrane [54] for up to 8 days [55]. Their overall charge was a sum of the individual charges contributed by each component; nevertheless, they were biocompatible and did not interfere with cell functions, such as cellular viability, differentiation, proliferation, and phenotype, nor did they cause inflammation or oxidative stress [54,56]. Using a magnetic drive (30 pN/cell) under a 24-well repellent culture plate (Greiner Bio-One, Kremsmünster, Austria) for up to 24 h, cells were plated with

Nanoshuttle-PL™ aggregate in the form of non-adherent spheroids that hold together even after magnet removal.

Briefly, adhered cells were washed with PBS, dissociated, centrifuged, and counted (cell viability was evaluated by Trypan Blue staining using a Neubauer chamber). Cells were suspended in DMEM/F-12 Glutamax (Gibco™, Waltham, MA, USA) completed with 10% fetal bovine serum (FBS—Gibco™, Waltham, USA), 0.8% hydrocortisone (Sigma-Aldrich™, Gillingham, UK), and 1% antibiotics (Pen Strep, Gibco™, Waltham, MA, USA), and mixed with magnetic beads considering a standard ratio of 0.4 µL of Nanoshuttle-PL™ for every 10,000 cells (4×10^{-5} nanoparticles/cell). To promote the interaction between nanoparticles and cells, three centrifugation steps (1500 rpm for three minutes each) were performed, after which the resulting suspension was plated in a 24-well repellent plate for bioprinting for 24 h using the underlying magnetic drive, kept in an incubator at 5% of CO₂ and 37 °C. All experiments were conducted in triplicate. Figure 1 illustrates the steps of the spheroid formation method.

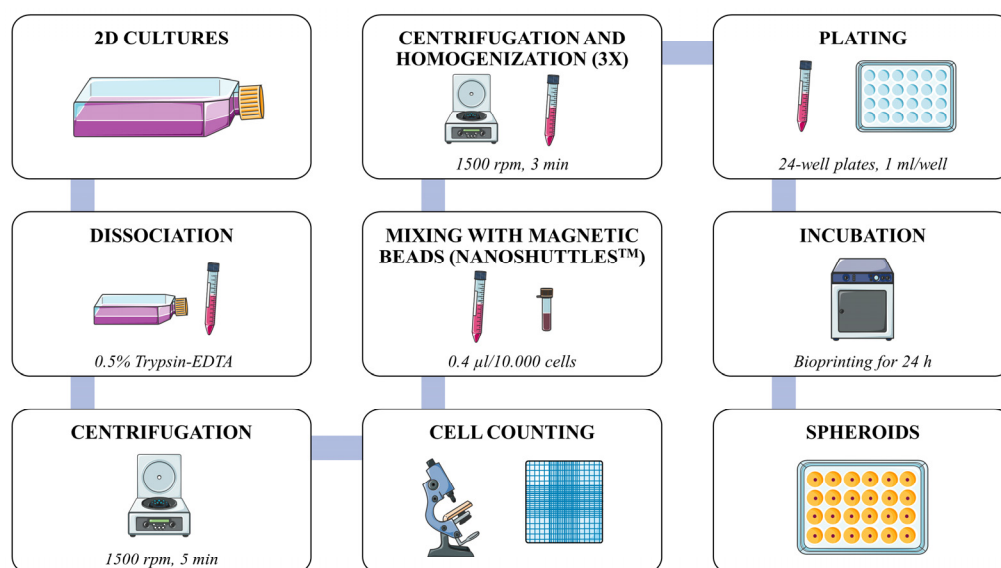


Figure 1. Flowchart of 3D bioprinted spheroid formation framework. Created using Smart Servier images (Creative Commons Attribution 3.0 France). Nanoshuttle-PL™ is a trademark of Greiner Bio-One.

2.3. Imaging and Analysis Parameters

Spheroids were plated in two groups (homotypic HSC3-only and heterotypic HSC3/CAF spheroids) at two cell densities (1×10^3 and 3×10^3 cells per well). Heterotypic spheroids were also cultured in two cell-type ratios (2:1 and 1:1 HSC3:CAF). All spheroids were monitored and analyzed at 6 h, 12 h, 48 h, and 72 h after plating. At every time point, cells were imaged using an Evos™ XL microscope (Thermo Scientific, Waltham, MA, USA) at 4× and 10× amplifications. The appraised parameters during imaging were spheroid size, evaluated by the largest diameter measured using ImageJ software version 1.8 (NIH, Bethesda, Rockville, MD, USA); spheroid form (roundness and cell density); distribution of cells between spheroid center and margin; and variability among replicates.

2.4. Histology and CIC Count

At 6 h, 12 h, 24 h, 48 h, and 72 h, two spheroids were collected from each experiment for histological processing. Briefly, plating media was removed from the well, and spheroids were collected using previously cut 1000 µL tips to avoid fragmentation. Each spheroid was kept in cold formaldehyde at 4% for at least 24 h, followed by paraffin embedding and sectioning into 4 µm slices. Sections were mounted onto slides and scanned using an Axio Imager Z2/VSLIDE Scanner (Zeiss Microscopy, Oberkochen, Germany). Analyses

were made using the OlyVIA visualizer version 2.4 (Olympus Lifescience, Tokyo, Japan). In addition, Supplementary Figure S1 shows the histological features of oral squamous cell carcinoma tissue.

For histomorphological analysis, the following aspects were considered [57,58] (Figure 2): tumoral zones (central/necrotic and marginal/proliferative), pleomorphism, and atypical cellular findings, visualization and location of CIC structures, identified by the morphological definition of “bird’s eye” or “signet ring” cells [15,59], i.e., outer cell well or partially outlined with a semilunar nucleus pushed towards the cellular periphery [60,61].

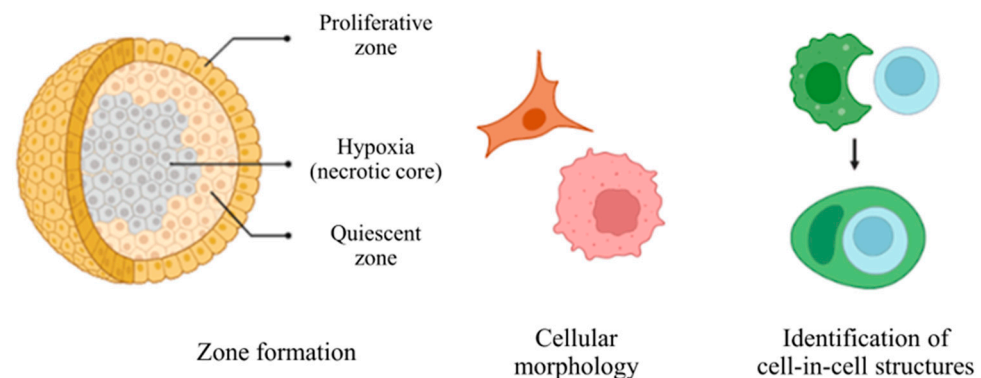


Figure 2. Representation of histomorphological features observed during H&E analysis. Created using Biorender.com (accessed on 30 April 2023).

Semiquantitative analysis was performed in sections obtained from $40\times$ amplified scanned slides. To count the CIC structures, one section from each of the two spheroids was selected from each group (homotypical and heterotypical) at each time point. For each sample, areas of $181\ \mu\text{m} \times 97\ \mu\text{m}$ were chosen randomly from each zone: one area from the spheroid margin (periphery) and one from the spheroid inner core (central). Results were expressed as a percentage corresponding to the number of CIC structures/total number of well-defined cells in the area. Analyses were performed using ImageJ software version 1.8 (NIH, Bethesda, USA).

2.5. Statistical Analysis

Results were analyzed using GraphPad Prism version 8 (Dotmatics, Boston, MA, USA). Data were evaluated for normality and Gaussian distribution, with parametric and nonparametric tests applied accordingly (Mann–Whitney test and Student’s *t*-Test). When determining differences between the two independent groups by comparing three or more independent groups, the *p*-value was considered less or equal to 5% for sampling variability.

3. Results

3.1. Spheroid Model Establishment

After plating, spheroids were monitored after 6 h, 12 h, 24 h, 48 h, and 72 h, while bioprinting was performed for 24 h (Figure 3A). Round-shaped spheroids with dense cellular aggregation at their center were seen from 6 h (Figure 3B). At 6 h, 12 h, and 24 h, heterotypic spheroids had a significantly larger diameter ($p = 0.025$), while a trend of time-dependent reduction in spheroid size (contraction) under all conditions was noted. This only reached statistical significance in the heterotypic spheroid group at 12 h (Figure 4). High reproducibility was also observed between the samples.

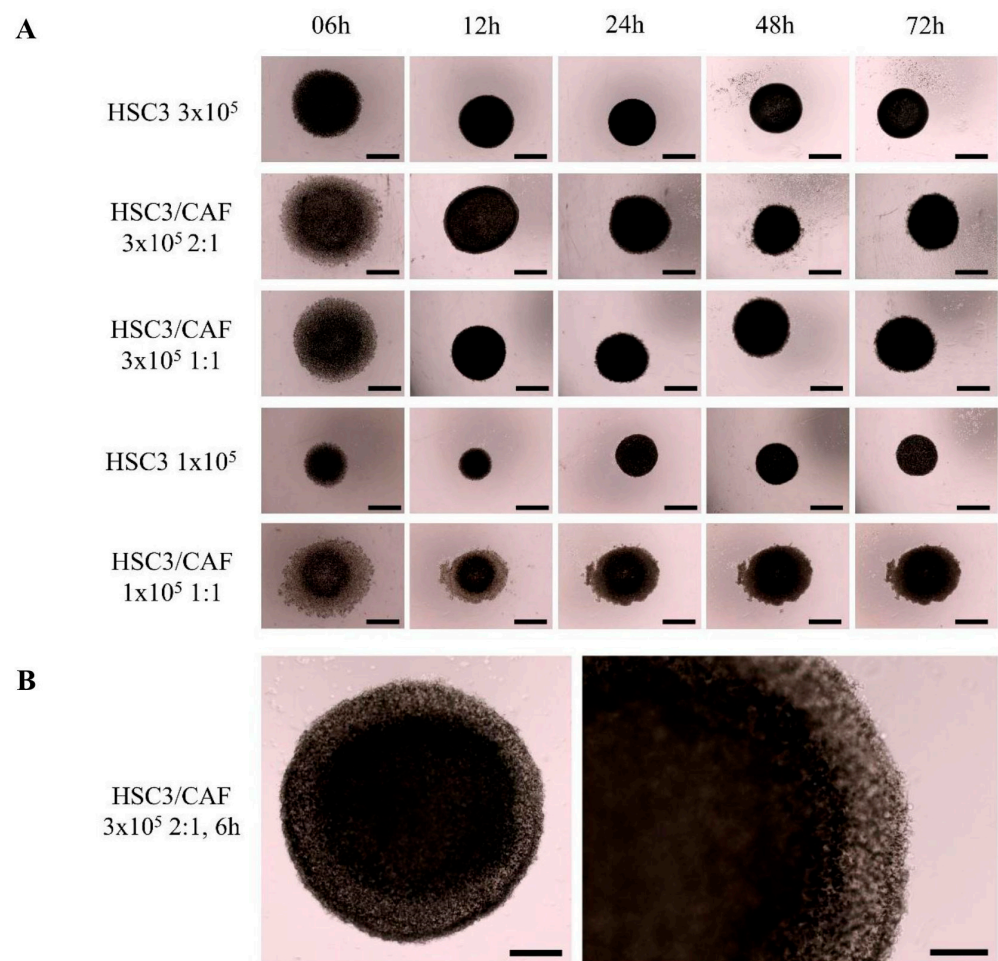


Figure 3. Oral squamous cell carcinoma (HSC3 line) homotypic and heterotypic (co-cultured with cancer-associated fibroblasts, CAF) spheroids. (A) Representative images of spheroids obtained with different cell plating densities, cell line combinations, and ratios (lines), taken at different timepoints (from the start of the 24 h bioprinting) (columns). At 6 h, spheroid formation can already be seen, reaching appropriate cell aggregation after 24 h. Images obtained with Evos™ XL. Scale bar: 1000 µm. (B) Representative images of cell organization. A central region with higher cell density can be seen, surrounded by an outer layer of sparse cellular organization, typical of a proliferative zone. Images obtained using Evos™ XL. Scale bar: 500 µm (left) and 250 µm (right).

3.2. Histomorphological Assessment

Histomorphological analysis using hematoxylin and eosin staining showed a spheroid morphology compatible with the formation of OSCC tumor zones, which can be further observed in the samples of OSCC tissues (Supplementary Figure S1). Tumor cells exhibited high pleomorphic and polyhedral aspects, consistent with the OSCC pattern (Figure 5A), whereas at the periphery of the spheroid (outer boundary), cells were cohesive and had a flatter shape (Figure 5B). In the heterotypic spheroids, we observed fusiform and elongated cells with a fibroblast-like morphology (Figure 5C). A necrotic center was observed in all groups, characterized by an amorphous area of eosinophilic staining and apoptotic cells. In homotypic spheroids, the necrotic center was predominantly singular, whereas in heterotypic groups, the presence of multiple sparse necrotic areas was noted (Figure 6A). Cellular pleomorphism and nuclear hyperchromatism were more evident in the proliferative zone (at the periphery of the spheroid). Furthermore, we observed areas of cellular loosening, starting from the edge of the spheroid (Figure 6B).

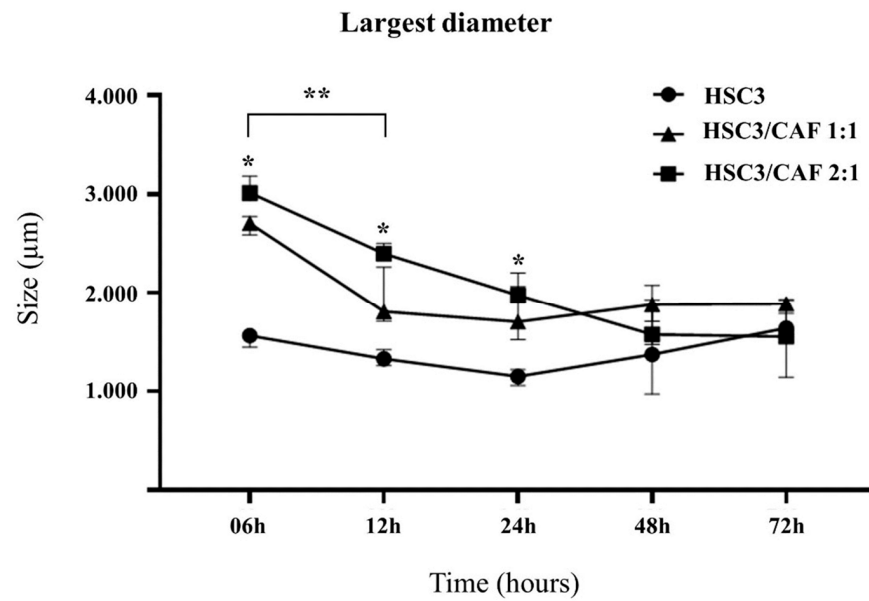


Figure 4. Median and standard deviation of spheroid diameter of homotypic and heterotypic groups (co-cultured with cancer-associated fibroblasts, CAF) in the evaluated timepoints. * Spheroid size in the heterotypic group size was bigger than in the homotypic group at 6 h, 12 h, and 24 h. ** Spheroid contraction was larger at 12 h. Image made with GraphPad Prism version 8.

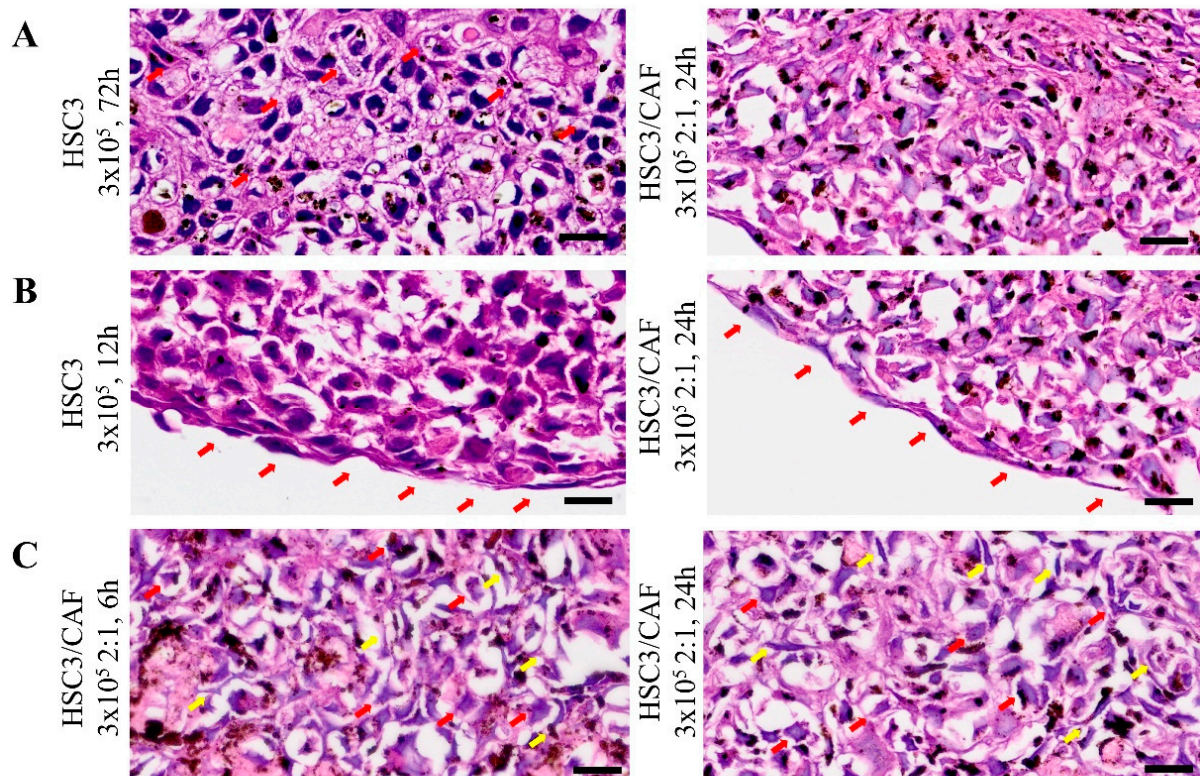


Figure 5. Histomorphological findings in 4 μm thickness sections obtained from oral squamous cell carcinoma (HSC3 line) spheroids, both homotypic and heterotypic (co-cultured with cancer-associated fibroblasts, CAF). (A) Pleomorphism seen in the tumor cell population and the formation of intercellular bridges can be seen (red arrows). (B) In the periphery of the spheroid, cells with a flatter morphology can be observed (red arrows). (C) Heterogeneous grouping of polyhedral cells (red arrows) and fusiform and elongated cells (yellow arrows). Images obtained using Axio Imager Z2/VSLIDE. Coloring: H/E. Scale bar: 20 μm .

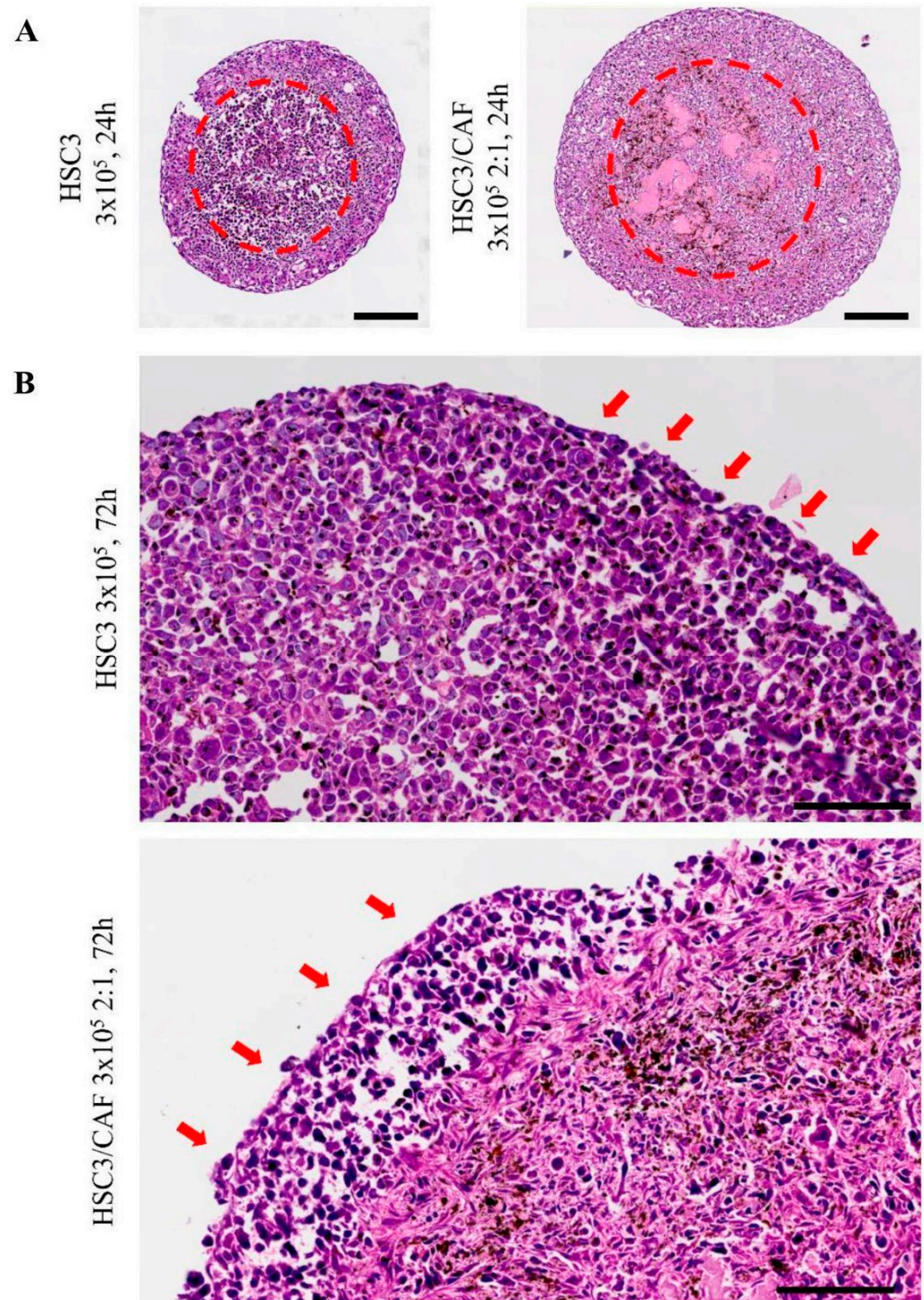


Figure 6. Histomorphological aspects in 4 μ m thickness sections obtained from oral squamous cell carcinoma (HSC3 line) spheroids, both homotypic and heterotypic (co-cultured with cancer-associated fibroblasts, CAF). **(A)** Necrotic cores (dotted red line) formed in homotypic (**left**) and heterotypic (**right**) spheroids. In the homotypical groups, the loss of cellular adhesion and tissue pattern suggest liquefactive necrosis. In mixed spheroids, multiple focal amorphous and eosinophilic areas were noticed, due to a difference in extracellular matrix deposition, and suggest a pattern of ischemic necrosis. Scale bar: 200 μ m. **(B)** Towards the periphery of the spheroid, a pattern of loss of cellular adhesion and hyperchromatic nuclei was frequent (red arrows), representative of necrotic cells. Images obtained using Axio Imager Z2/VSLIDE. Coloring: H/E. Scale bar: 200 μ m (**top**) and 100 μ m (**bottom**).

3.3. Identification of Cell-in-Cell Events

To assess the presence of CIC structures, the morphological description of “signet rings” or “bird’s eye cells” was defined as a parameter for the identification of these events. CIC structures were observed in all regions of both homotypic and heterotypic spheroids. In most cases, the outer cell’s nucleus presented a classic “spindle-shaped” form, whereas the inner cell’s nucleus was not always visible. Meanwhile, the cellular membranes of the involved cells did not always present visible continuity. These findings varied in size, roundness, integrity of the involved cells, and proximity to one another, sometimes appearing as clusters of CIC events (Figure 7). CIC structures were more abundant in the spheroids of HSC3 cells cultured with CAFs (Kruskal–Wallis, $p = 0.0037$ and 0.0464) (Figure 8A) and in proliferative areas (ANOVA, $p = 0.0062$), closer to the margin of the spheroids (Figure 8B). In some cases, engulfed cells were found within other internalized cells, a phenomenon that has been described as “complex cannibalism” [20] (Figure 9).

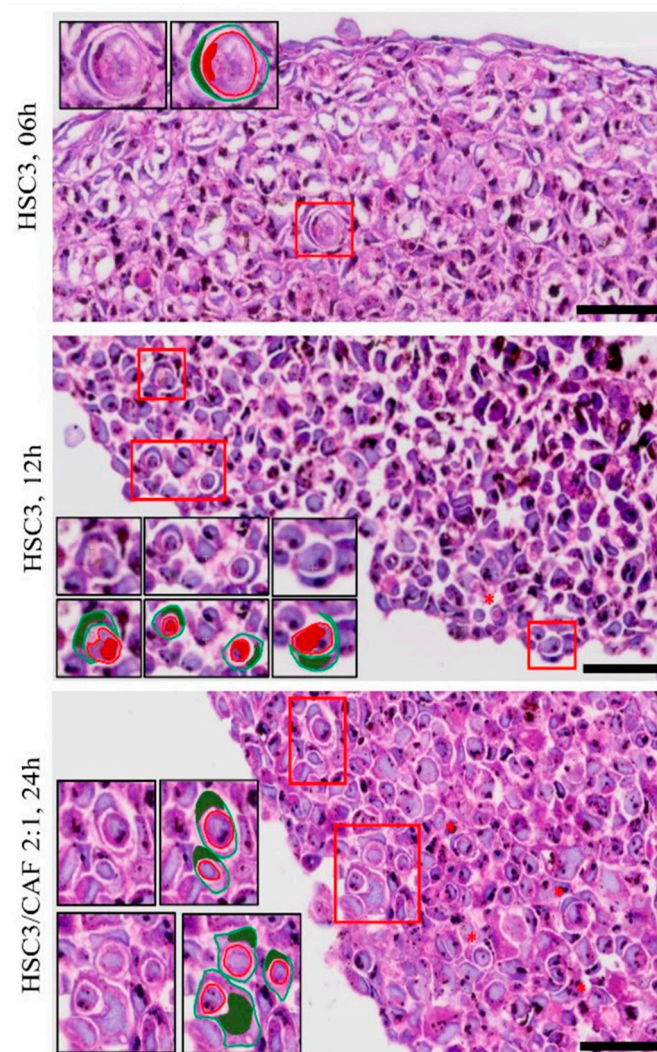


Figure 7. Cell-in-cell structures, described as “signet ring” or “bird’s eye” cells, found in 4 μ m thickness sections of homotypical and heterotypical spheroids of oral squamous cell carcinoma co-cultured with cancer-associated fibroblasts. Red asterisks indicate cell-in-cell structures and, in detail (red box), graphical representations of cell-in-cell structures (external cell and its nucleus in green, and internal cell with or without its nucleus shown in red). Image obtained using Axio Imager Z2/VSLIDE. Graphic details made by the author. Coloring: H/E. Scale bar: 20 μ m. CAF = cancer-associated fibroblasts.

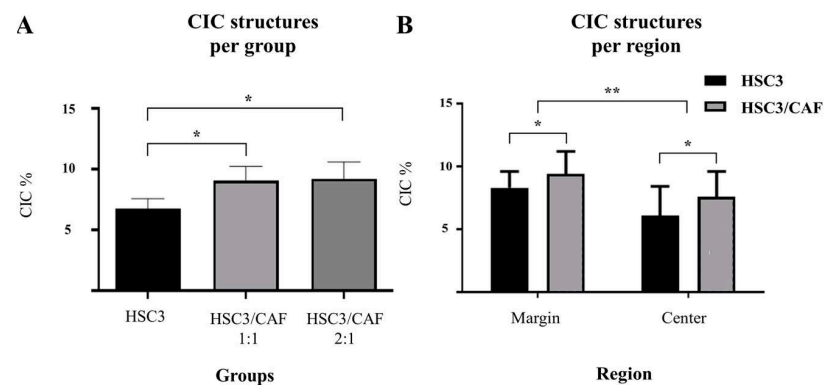


Figure 8. Data on cell-in-cell structures found in oral squamous cell carcinoma spheroids, both homotypical and heterotypical (co-cultured with cancer-associated fibroblasts, CAF), expressed in percentage of total cell-in-cell structures per total amount of cells detected within a predefined region. (A) Cell-in-cell (CIC) structures were more frequent in heterotypic spheroids (*). (B) Cell-in-cell structures were more frequent in the periphery (proliferative zone) and center (necrotic core) of heterotypic spheroids (*), and, in both groups (homotypic and heterotypic), more structures were found in the proliferative zone (**). Images made with GraphPad Prism version 8.

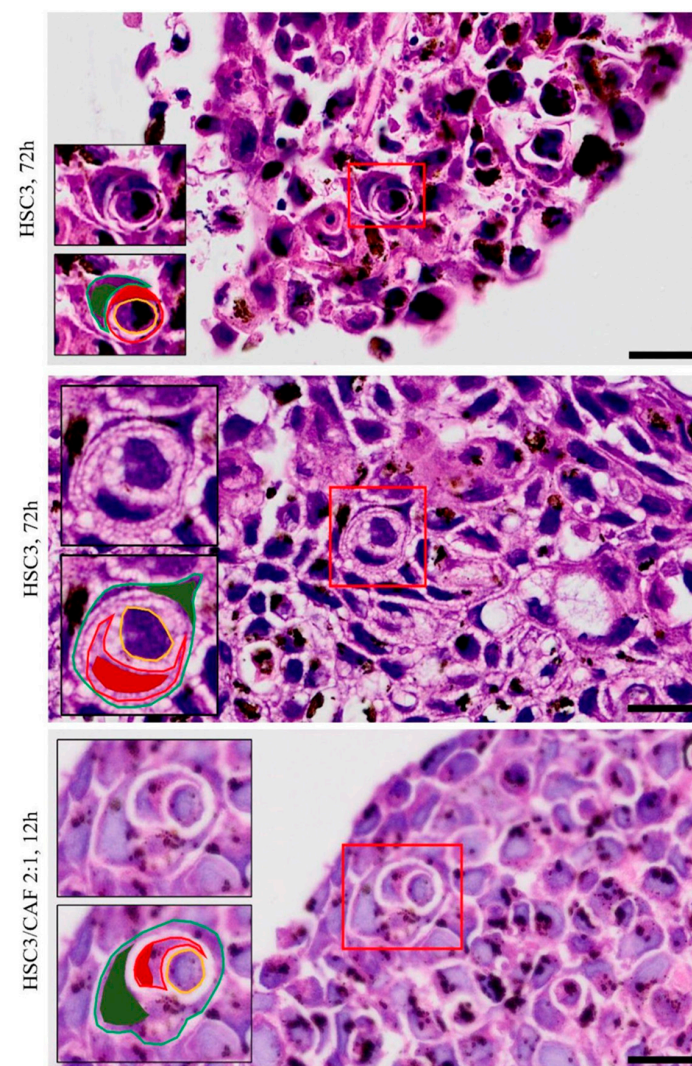


Figure 9. Cell-in-cell structures, described as “complex cannibalism”, in which a cell is found within a cell within another cell, found in 4 μ m thickness sections of homotypical and heterotypical spheroids

of oral squamous cell carcinoma co-cultured with cancer-associated fibroblasts. In detail (red box), the outer cell, and its nucleus (in green), the “middle” cell and its nucleus (in red), and the inner cell (in yellow). Image obtained using Axio Imager Z2/VSLIDE. Graphic details made by the author. Coloring: H/E. Scale bar: 20 μ m. CAF = cancer-associated fibroblasts.

4. Discussion

Since the first reports of CIC findings were made over 100 years ago [17,62,63], they have become common findings in malignancies such as lung cancer [64], breast cancer [11,65], and oral cancer [12,66], and have been linked to an increase in tumor aggressiveness [67,68], resistance [22] and survival [69–71], leading to worse prognosis [25,72]. However, despite being easily identifiable in routine H/E stains and electron microscopy [69,73–76], there is a need for models that enable further study of these events in vitro. Herein, we demonstrate that CIC structures can be studied in 3D bioprinted spheroids, which reproduce histomorphological features of the OSCC.

Despite bioprinting spheroids having been used to study various cancer types such as glioblastoma [53,77], breast cancer [78], pancreatic duct adenocarcinoma [55], osteosarcoma [79] and ovarian cancer [80], there is a lack of studies that validate this model for OSCC. The spheroid bioprinting method might represent an advantageous approach compared to hanging drop cultures [81], organ-on-a-chip [82], and organoids [83] for allowing higher reproducibility, technical simplicity, and the ability to construct heterotypic spheroids with well-nutrient distribution and tumor zone formation [84–86]. This approach cooperates in dealing with the lack of appropriate methods to study CIC structures [11,18,87]. Meanwhile, the reproduction of heterotypic cell–cell interactions, heterogeneous distribution of oxygen, and consequently the formation of tumor zones [55,88,89], all of which influence the formation of CIC structures [18,30], confer an advantage to the use of spheroid models in this field.

Despite no correlation between CIC frequency and time of observation, our findings show that CIC structures were more frequent in the proliferative zone of heterotypic OSCC/CAF spheroids. The occurrence of heterotypical interactions involving mesenchymal and cancer cells in spheroids has been described in breast cancer [11,90] and pancreatic cancer [85], but not to the best of our knowledge in OSCC. CIC findings have been associated with aggressiveness hallmarks, such as cell invasion and resistance [26,91], as well as stemness [92,93]. In addition, it is well established that CAFs play an essential role in tumor metabolism [31,32], invasion and metastasis [94–96], autophagy [97], and therapeutic resistance [98]. Further immunophenotyping studies using spheroid sections may be helpful in matching CAF and CIC identification with the expression of markers such as NANOG and SOX2, considering their confluent association with tumor prognosis [11,92,93]. Additionally, given the production of the extracellular matrix by HSC3 cells [99] and the role of CAFs in remodeling such matrix [31,32], it is important that further studies investigate the role of cellular–matrix interactions in the formation of CIC structures.

Despite cellular interactions being ubiquitous [100], in our results, CIC structures appeared more often in the proliferative zone. It is important to emphasize that within this tumor microenvironment model, cancer cells exhibit enhanced plasticity and an invasive phenotype [57,101,102]. Meanwhile, previous studies show that the fibroblasts are predominantly located in the periphery of the spheroids [103,104], which could further suggest the participation of these cells in CIC formation. In contrast, some studies indicate hypoxia as a relevant aspect for triggering the formation of CIC [21,26] due to its relationship with tumor metabolism [105,106]. Nevertheless, it is important to acknowledge that the conventional histomorphological characterization of CIC structures alone is inadequate in identifying the cell types involved in their formation, as well as if the involved cells are undergoing cell death [24,60,107], which could explain less detection of CIC features in necrotic zones, despite also having been observed in this study. Immunophenotyping assays can aid in cellular identification and in understanding the mechanisms behind the located CIC events (e.g., cannibalism and entosis).

In summary, in this study, we employed a spheroid bioprinting method to study CIC events in oral cancer for the first time. CIC was detected throughout the spheroids but more commonly in the proliferative area of spheroids in which cancer cells were cocultured with CAFs. This study demonstrates that the spheroid bioprinting model described here offers a reliable and practical approach for studying the mechanisms underpinning the formation of CIC structures; this may lead to the identification of prognosis biomarkers and possible therapeutic targets in translational oncology.

Supplementary Materials: The following supporting information can be downloaded at: <https://www.mdpi.com/article/10.3390/cells12192418/s1>, Figure S1. Histomorphological aspects of oral squamous cell carcinoma. Islands of epithelial cells exhibiting polyhedral format with intercellular bridges. Especially in the periphery of the tumor islands, we also observe cells in a fusiform pattern. Cellular hyperchromatism (red arrows) and clear cytoplasm (*) may also be observed. Magnification: 400×.

Author Contributions: Conceptualization, L.d.O.S.d.R., B.S.d.F.S., D.W.L. and C.A.G.R.; methodology, L.d.O.S.d.R., B.S.d.F.S., R.D.C., D.W.L. and C.A.G.R.; validation, L.d.O.S.d.R.; formal analysis, L.d.O.S.d.R., D.W.L. and C.A.G.R.; investigation, L.d.O.S.d.R. and C.A.G.R.; resources, B.S.d.F.S., R.D.C., D.W.L. and C.A.G.R.; data curation, R.D.C., D.W.L. and C.A.G.R.; writing—original draft preparation, L.d.O.S.d.R. and C.A.G.R.; writing—review and editing, L.d.O.S.d.R., D.W.L. and C.A.G.R.; visualization, L.d.O.S.d.R., B.S.d.F.S., R.D.C., D.W.L. and C.A.G.R.; supervision, B.S.d.F.S., D.W.L. and C.A.G.R.; project administration, B.S.d.F.S., R.D.C., D.W.L. and C.A.G.R.; funding acquisition, C.A.G.R. All authors have read and agreed to the published version of the manuscript.

Funding: This research was funded by the Academy of Medical Sciences/Newton Advanced Fellowship Grant (NAFR12\1035), the Brazilian research financial institution the National Council for Scientific and Technological Development (CNPq) (308276/2019-1), and the Program for Excellence in Research of the Oswaldo Cruz Foundation (PROEP-FIOCRUZ-BA) (02.385.669/0001-74, ID 2034).

Institutional Review Board Statement: The study was conducted in accordance with the Declaration of Helsinki and approved by the Ethics Committee of The School of Dentistry of the University of Campinas (protocol code 4.706.681, 12 May 2021).

Informed Consent Statement: Not applicable.

Data Availability Statement: The data presented in this study are available on request from the corresponding author.

Acknowledgments: The authors would like to thank the Service of Histopathology and the Service of Microscopy at the Gonçalo Moniz Institute (FIOCRUZ-BA), as well as Roquelina Assis and the team at the Center of Biotechnology and Cellular Therapy, for their technical support.

Conflicts of Interest: The authors declare no conflict of interest. The funders had no role in the design of the study; in the collection, analyses, or interpretation of data; in the writing of the manuscript; or in the decision to publish the results.

References

1. World Health Organization. *Global Oral Health Status Report: Towards Universal Health Coverage for Oral Health by 2030*; World Health Organization: Geneva, Switzerland, 2022.
2. Bavle, R.M.; Venugopal, R.; Konda, P.; Muniswamappa, S.; Makarla, S. Molecular Classification of Oral Squamous Cell Carcinoma. *J. Clin. Diagn. Res.* **2016**, *10*, ZE18. [[CrossRef](#)] [[PubMed](#)]
3. INCA. *Estimativa 2020: Incidência de Câncer No Brasil*; INCA: Rio de Janeiro, Brazil, 2019.
4. El-Naggar, A.K.; Chan, J.K.C.; Grandis, J.R.; Takata, T.; Slootweg, P.J. *WHO Classification of Head and Neck Tumours*; World Health Organization: Geneva, Switzerland, 2017.
5. Gondivkar, S.M.; Gadgil, A.R.; Sarode, S.C.; Hedao, A.; Dasgupta, S.; Sharma, B.; Sharma, A.; Gondivkar, R.S.; Yuwanati, M.; Patil, S.; et al. Oral and general health-related quality of life in oral squamous cell carcinoma patients- comparative analysis of different treatment regimens. *J. Oral Biol. Craniofacial Res.* **2021**, *11*, 125–131. [[CrossRef](#)] [[PubMed](#)]
6. Louredo, B.V.R.; Vargas, P.A.; Pérez-De-oliveira, M.E.; Lopes, M.A.; Kowalski, L.P.; Curado, M.P. Epidemiology and survival outcomes of lip, oral cavity, and oropharyngeal squamous cell carcinoma in a southeast Brazilian population. *Med. Oral Patol. Oral Cir. Bucal* **2022**, *27*, e274. [[CrossRef](#)]

7. Jubelin, C.; Muñoz-Garcia, J.; Griscom, L.; Cochonneau, D.; Ollivier, E.; Heymann, M.F.; Vallette, F.M.; Oliver, L.; Heymann, D. Three-dimensional in vitro culture models in oncology research. *Cell Biosci.* **2022**, *12*, 155. [\[CrossRef\]](#)
8. Kim, J.; Park, C.; Kim, K.H.; Kim, E.H.; Kim, H.; Woo, J.K.; Seong, J.K.; Nam, K.T.; Lee, Y.C.; Cho, S.Y. Single-cell analysis of gastric pre-cancerous and cancer lesions reveals cell lineage diversity and intratumoral heterogeneity. *NPJ Precis. Oncol.* **2022**, *6*, 9. [\[CrossRef\]](#) [\[PubMed\]](#)
9. Molina, M.F.; Fabre, T.; Cleret-Buhot, A.; Soucy, G.; Meunier, L.; Abdelnabi, M.N.; Belforte, N.; Turcotte, S.; Shoukry, N.H. Visualization, Quantification, and Mapping of Immune Cell Populations in the Tumor Microenvironment. *J. Vis. Exp.* **2020**, *157*, e60740. [\[CrossRef\]](#)
10. Choe, C.; Shin, Y.S.; Kim, S.H.; Jeon, M.J.; Choi, S.J.; Lee, J.; Kim, J. Tumor-stromal interactions with direct cell contacts enhance motility of non-small cell lung cancer cells through the hedgehog signaling pathway. *Anticancer Res.* **2013**, *33*, 3715–3724.
11. Bartosh, T.J.; Ullah, M.; Zeitouni, S.; Beaver, J.; Prockop, D.J. Cancer cells enter dormancy after cannibalizing mesenchymal stem/stromal cells (MSCs). *Proc. Natl. Acad. Sci. USA* **2016**, *113*, E6447–E6456. [\[CrossRef\]](#)
12. Almangush, A.; Mäkitie, A.A.; Hagström, J.; Haglund, C.; Kowalski, L.P.; Nieminen, P.; Coletta, R.D.; Salo, T.; Leivo, I. Cell-in-cell phenomenon associates with aggressive characteristics and cancer-related mortality in early oral tongue cancer. *BMC Cancer* **2020**, *20*, 843. [\[CrossRef\]](#)
13. Sarode, G.S.; Sarode, S.C.; Karmarkar, S. Complex cannibalism: An unusual finding in oral squamous cell carcinoma. *Oral Oncol.* **2012**, *48*, e4. [\[CrossRef\]](#)
14. Bauchwitz, M. The Bird's eye cell: Cannibalism or abnormal division of tumor cells. *Acta Cytol.* **1981**, *25*, 92.
15. Breier, F.; Feldmann, R.; Fellenz, C.; Neuhold, N.; Gschnait, F. Primary invasive signet-ring cell melanoma. *J. Cutan. Pathol.* **1999**, *26*, 533–536. [\[CrossRef\]](#)
16. Martinez, V.; Azzopardi, J.G. Invasive lobular carcinoma of the breast: Incidence and variants. *Histopathology* **1979**, *3*, 467–488. [\[CrossRef\]](#) [\[PubMed\]](#)
17. Steinhaus, J. Ueber carcinoma-einschlusse. *Virchows Arch.* **1891**, *126*, 533–535. [\[CrossRef\]](#)
18. Siquara da Rocha, L.d.O.; Souza, B.S.d.F.; Lambert, D.W.; Gurgel Rocha, C.d.A. Cell-in-Cell Events in Oral Squamous Cell Carcinoma. *Front. Oncol.* **2022**, *12*, 931092. [\[CrossRef\]](#) [\[PubMed\]](#)
19. Fais, S. A role for ezrin in a neglected metastatic tumor function. *Trends Mol. Med.* **2004**, *10*, 249–250. [\[CrossRef\]](#)
20. Sarode, S.C.; Sarode, G.S. Neutrophil-tumor cell cannibalism in oral squamous cell carcinoma. *J. Oral Pathol. Med.* **2014**, *43*, 454–458. [\[CrossRef\]](#)
21. Meléndez-Lazo, A.; Cazzini, P.; Camus, M.; Doria-Torra, G.; Marco Valle, A.J.; Solano-Gallego, L.; Pastor, J. Cell cannibalism by malignant neoplastic cells: Three cases in dogs and a literature review. *Vet. Clin. Pathol.* **2015**, *44*, 287–294. [\[CrossRef\]](#)
22. Ruan, B.; Wang, C.; Chen, A.; Liang, J.; Niu, Z.; Zheng, Y.; Fan, J.; Gao, L.; Huang, H.; Wang, X.; et al. Expression profiling identified IL-8 as a regulator of homotypic cell-in-cell formation. *BMB Rep.* **2018**, *51*, 412–417. [\[CrossRef\]](#)
23. Tonnessen-Murray, C.A.; Frey, W.D.; Rao, S.G.; Shahbandi, A.; Ungerleider, N.A.; Olayiwola, J.O.; Murray, L.B.; Vinson, B.T.; Chrisey, D.B.; Lord, C.J.; et al. Chemotherapy-induced senescent cancer cells engulf other cells to enhance their survival. *J. Cell Biol.* **2019**, *218*, 3827–3844. [\[CrossRef\]](#)
24. Mackay, H.L.; Muller, P.A.J. Biological relevance of cell-in-cell in cancers. *Biochem. Soc. Trans.* **2019**, *47*, 725–732. [\[CrossRef\]](#) [\[PubMed\]](#)
25. Gottwald, D.; Putz, F.; Hohmann, N.; Büttner-Herold, M.; Hecht, M.; Fietkau, R.; Distel, L. Role of tumor cell senescence in non-professional phagocytosis and cell-in-cell structure formation. *BMC Mol. Cell Biol.* **2020**, *21*, 79. [\[CrossRef\]](#) [\[PubMed\]](#)
26. Siddiqui, S.; Singh, A.; Faizi, N.; Khalid, A. Cell cannibalism in oral cancer: A sign of aggressiveness, de-evolution, and retroversion of multicellularity. *J. Cancer Res. Ther.* **2019**, *15*, 631–637. [\[CrossRef\]](#) [\[PubMed\]](#)
27. Sun, Q.; Huang, H.; Overholtzer, M. Cell-in-cell structures are involved in the competition between cells in human tumors. *Mol. Cell Oncol.* **2015**, *2*, 2014–2016. [\[CrossRef\]](#) [\[PubMed\]](#)
28. Anderson, N.M.; Simon, M.C. The tumor microenvironment. *Curr. Biol.* **2020**, *30*, R921–R925. [\[CrossRef\]](#) [\[PubMed\]](#)
29. Baghban, R.; Roshangar, L.; Jahanban-Esfahlan, R.; Seidi, K.; Ebrahimi-Kalan, A.; Jaymand, M.; Kolahian, S.; Javaheri, T.; Zare, P. Tumor microenvironment complexity and therapeutic implications at a glance. *Cell Commun. Signal.* **2020**, *18*, 59. [\[CrossRef\]](#)
30. Wang, X.; Li, Y.; Li, J.; Li, L.; Zhu, H.; Chen, H.; Kong, R.; Wang, G.; Wang, Y.; Hu, J.; et al. Cell-in-Cell Phenomenon and Its Relationship with Tumor Microenvironment and Tumor Progression: A Review. *Front. Cell Dev. Biol.* **2019**, *7*, 311. [\[CrossRef\]](#)
31. Peng, S.; Chen, D.; Cai, J.; Yuan, Z.; Huang, B.; Li, Y.; Wang, H.; Luo, Q.; Kuang, Y.; Liang, W.; et al. Enhancing cancer-associated fibroblast fatty acid catabolism within a metabolically challenging tumor microenvironment drives colon cancer peritoneal metastasis. *Mol. Oncol.* **2021**, *15*, 1391–1411. [\[CrossRef\]](#)
32. Yang, J.; Shi, X.; Yang, M.; Luo, J.; Gao, Q.; Wang, X.; Wu, Y.; Tian, Y.; Wu, F.; Zhou, H. Glycolysis reprogramming in cancer-associated fibroblasts promotes the growth of oral cancer through the lncRNA H19/miR-675-5p/PFKFB3 signaling pathway. *Int. J. Oral Sci.* **2021**, *13*, 12. [\[CrossRef\]](#)
33. Mellone, M.; Hanley, C.J.; Thirdborough, S.; Mellows, T.; Garcia, E.; Woo, J.; Tod, J.; Frampton, S.; Jenei, V.; Moutasim, K.A.; et al. Induction of fibroblast senescence generates a non-fibroblastic myofibroblast phenotype that differentially impacts on cancer prognosis. *Aging* **2017**, *9*, 114. [\[CrossRef\]](#)
34. Matte, B.F.; Kumar, A.; Placone, J.K.; Zanella, V.G.; Martins, M.D.; Engler, A.J.; Lamers, M.L. Matrix stiffness mechanically conditions EMT and migratory behavior of oral squamous cell carcinoma. *J. Cell Sci.* **2019**, *132*, jcs224360. [\[CrossRef\]](#) [\[PubMed\]](#)

35. de Bem Prunes, B.; Nunes, J.S.; da Silva, V.P.; Laureano, N.K.; Gonçalves, D.R.; Machado, I.S.; Barbosa, S.; Lamers, M.L.; Rados, P.V.; Kurth, I.; et al. The role of tumor acidification in aggressiveness, cell dissemination and treatment resistance of oral squamous cell carcinoma. *Life Sci.* **2022**, *288*, 120163. [[CrossRef](#)] [[PubMed](#)]
36. Niklander, S.E.; Lambert, D.W.; Hunter, K.D. Senescent Cells in Cancer: Wanted or Unwanted Citizens. *Cells* **2021**, *10*, 3315. [[CrossRef](#)]
37. Saito, K.; Mitsui, A.; Sumardika, I.W.; Yokoyama, Y.; Sakaguchi, M.; Kondo, E. PLOD2-driven IL-6/STAT3 signaling promotes the invasion and metastasis of oral squamous cell carcinoma via activation of integrin β 1. *Int. J. Oncol.* **2021**, *58*, 29. [[CrossRef](#)] [[PubMed](#)]
38. Deng, Z.; Wang, H.; Liu, J.; Deng, Y.; Zhang, N. Comprehensive understanding of anchorage-independent survival and its implication in cancer metastasis. *Cell Death Dis.* **2021**, *12*, 629. [[CrossRef](#)] [[PubMed](#)]
39. Reinfeld, B.I.; Madden, M.Z.; Wolf, M.M.; Chytil, A.; Bader, J.E.; Patterson, A.R.; Sugiura, A.; Cohen, A.S.; Ali, A.; Do, B.T.; et al. Cell Programmed Nutrient Partitioning in the Tumor Microenvironment. *Nature* **2021**, *593*, 282. [[CrossRef](#)] [[PubMed](#)]
40. Vaziri-Gohar, A.; Cassel, J.; Mohammed, F.S.; Zarei, M.; Hue, J.J.; Hajihassani, O.; Graor, H.J.; Srikanth, Y.V.V.; Karim, S.A.; Abbas, A.; et al. Limited nutrient availability in the tumor microenvironment renders pancreatic tumors sensitive to allosteric IDH1 inhibitors. *Nat. Cancer* **2022**, *3*, 852–865. [[CrossRef](#)]
41. Khayatan, D.; Hussain, A.; Tebyaniyan, H. Exploring animal models in oral cancer research and clinical intervention: A critical review. *Vet. Med. Sci.* **2023**, *9*, 1833–1847. [[CrossRef](#)]
42. Peng, S.; Creighton, C.J.; Zhang, Y.; Sen, B.; Mazumdar, T.; Myers, J.N.; Woolfson, A.; Lorenzi, M.V.; Bell, D.; Williams, M.D.; et al. Tumor grafts derived from patients with head and neck squamous carcinoma authentically maintain the molecular and histologic characteristics of human cancers. *J. Transl. Med.* **2013**, *11*, 198. [[CrossRef](#)]
43. Ahmed, M.A.M.; Nagelkerke, A. Current developments in modelling the tumour microenvironment in vitro: Incorporation of biochemical and physical gradients. *Organs-Chip* **2021**, *3*, 100012. [[CrossRef](#)]
44. Emami Nejad, A.; Najafgholian, S.; Rostami, A.; Sistani, A.; Shojaeifar, S.; Esparvarinha, M.; Nedaeinia, R.; Javanmard, S.H.; Taherian, M.; Ahmadi, M.; et al. The role of hypoxia in the tumor microenvironment and development of cancer stem cell: A novel approach to developing treatment. *Cancer Cell Int.* **2021**, *21*, 62. [[CrossRef](#)] [[PubMed](#)]
45. Li, Y.; Zhao, L.; Li, X.F. Hypoxia and the Tumor Microenvironment. *Technol. Cancer Res. Treat.* **2021**, *20*, 15330338211036304. [[CrossRef](#)] [[PubMed](#)]
46. Petrova, V.; Annicchiarico-Petruzzelli, M.; Melino, G.; Amelio, I. The hypoxic tumour microenvironment. *Oncogenesis* **2018**, *7*, 10. [[CrossRef](#)] [[PubMed](#)]
47. Calar, K.; Plesselova, S.; Bhattacharya, S.; Jorgensen, M.; de la Puente, P. Human Plasma-Derived 3D Cultures Model Breast Cancer Treatment Responses and Predict Clinically Effective Drug Treatment Concentrations. *Cancers* **2020**, *12*, 1722. [[CrossRef](#)]
48. Vidavsky, N.; Kunitake, J.A.; Chiou, A.E.; Northrup, P.A.; Porri, T.J.; Ling, L.; Fischbach, C.; Estroff, L.A. Studying biomineralization pathways in a 3D culture model of breast cancer microcalcifications. *Biomaterials* **2018**, *179*, 71–82. [[CrossRef](#)]
49. Filipiak-Duliban, A.; Brodaczewska, K.; Majewska, A.; Kieda, C. Spheroid culture models adequately imitate distinctive features of the renal cancer or melanoma microenvironment. *Vitr. Cell Dev. Biol. Anim.* **2022**, *58*, 349–364. [[CrossRef](#)]
50. Asthana, A.; Ndyabawe, K.; Mendez, D.; Douglass, M.; Haidekker, M.A.; Kisaalita, W.S. Calcium Oscillation Frequency Is a Potential Functional Complex Physiological Relevance Indicator for a Neuroblastoma-Based 3D Culture Model. *ACS Biomater. Sci. Eng.* **2020**, *6*, 4314–4323. [[CrossRef](#)]
51. Wang, Z.; Jiang, H.; Cai, L.Y.; Ji, N.; Zeng, X.; Zhou, Y.; Shen, Y.; Chen, Q. Repurposing disulfiram to induce OSCC cell death by cristae dysfunction promoted autophagy. *Oral Dis.* **2021**, *27*, 1148–1160. [[CrossRef](#)]
52. Sobral, L.M.; Zecchin, K.G.; De Aquino, S.N.; Lopes, M.A.; Graner, E.; Coletta, R.D. Isolation and characterization of myofibroblast cell lines from oral squamous cell carcinoma. *Oncol. Rep.* **2011**, *25*, 1013–1020. [[CrossRef](#)]
53. Souza, G.R.; Molina, J.R.; Raphael, R.M.; Ozawa, M.G.; Stark, D.J.; Levin, C.S.; Bronk, L.F.; Ananta, J.S.; Mandelin, J.; Georgescu, M.-M.; et al. Three-dimensional tissue culture based on magnetic cell levitation. *Nat. Nanotechnol.* **2010**, *5*, 291–296. [[CrossRef](#)]
54. Caleffi, J.T.; Aal, M.C.E.; Gallindo, H.d.O.M.; Caxali, G.H.; Crulhas, B.P.; Ribeiro, A.O.; Souza, G.R.; Delella, F.K. Magnetic 3D cell culture: State of the art and current advances. *Life Sci.* **2021**, *286*, 120028. [[CrossRef](#)] [[PubMed](#)]
55. Ali, E.A.; Bordacahar, B.; Mestas, J.L.; Batteux, F.; Lafon, C.; Camus, M.; Prat, F. Ultrasonic cavitation induces necrosis and impairs growth in three-dimensional models of pancreatic ductal adenocarcinoma. *PLoS ONE* **2018**, *13*, e0209094. [[CrossRef](#)]
56. Gaitán-Salvatella, I.; López-Villegas, E.O.; González-Alva, P.; Susate-Olmos, F.; Álvarez-Pérez, M.A. Case Report: Formation of 3D Osteoblast Spheroid Under Magnetic Levitation for Bone Tissue Engineering. *Front. Mol. Biosci.* **2021**, *8*, 579. [[CrossRef](#)] [[PubMed](#)]
57. Malhão, F.; Macedo, A.C.; Ramos, A.A.; Rocha, E. Morphometrical, Morphological, and Immunocytochemical Characterization of a Tool for Cytotoxicity Research: 3D Cultures of Breast Cell Lines Grown in Ultra-Low Attachment Plates. *Toxics* **2022**, *10*, 415. [[CrossRef](#)] [[PubMed](#)]
58. Marques, I.A.; Fernandes, C.; Tavares, N.T.; Pires, A.S.; Abrantes, A.M.; Botelho, M.F. Magnetic-Based Human Tissue 3D Cell Culture: A Systematic Review. *Int. J. Mol. Sci.* **2022**, *23*, 12681. [[CrossRef](#)] [[PubMed](#)]
59. Hull, M.T.; Seo, I.S.; Battersby, J.S.; Csicsko, J.F. Signet-ring Cell Carcinoma of the Breast: A Clinicopathologic Study of 24 Cases. *Am. J. Clin. Pathol.* **1980**, *73*, 31–35. [[CrossRef](#)]

60. Borensztejn, K.; Tyrna, P.; Gawel, A.M.; Dziuba, I.; Wojcik, C.; Bialy, L.P.; Mlynarczuk-Bialy, I. Classification of cell-in-cell structures: Different phenomena with similar appearance. *Cells* **2021**, *10*, 2569. [\[CrossRef\]](#)
61. Overholtzer, M.; Brugge, J.S. The cell biology of cell-in-cell structures. *Nat. Rev. Mol. Cell Biol.* **2008**, *9*, 796–809. [\[CrossRef\]](#)
62. Eberth, J. Über die feineren bau der darmschleithaut. *Wurzb Naturwiss Zeitschr* **1864**, *5*, 11.
63. Stroebe, H. *Zur Kenntniss Verschiedener Cellularer Vorgänge und Erscheinungen in Geschwulsten*; Gustav Fischer: Portland, OR, USA, 1890; Volume 10.
64. DeSimone, P.A.; East, R.; Powell, R.D. Phagocytic tumor cell activity in oat cell carcinoma of the lung. *Hum. Pathol.* **1980**, *11*, 535–539.
65. Fujii, M.; Ishii, Y.; Wakabayashi, T.; Itoyanagi, N.; Hagiwara, K.; Saito, M.; Takahashi, M. Cytologic diagnosis of male breast cancer with nipple discharge. A case report. *Acta Cytol.* **1986**, *30*, 21–24.
66. Jain, M.; Saawarn, S.; Gupta, A.; Ashok, S.; Mhaske, S.; Khan, S.; Jain, M. Assessment of Tumor Cell Cannibalism as a Predictor of Oral Squamous Cell Carcinoma—A Histopathologic Correlation. *Gulf J. Oncol.* **2017**, *1*, 52–56.
67. Suwasini, M.S.; Kumar, M. Assesment of Cellular Cannibalism in Predicting the Aggressive Nature of Oral Squamous Cell Carcinoma. *Int. J. Curr. Adv. Res.* **2020**, *9*, 9–12.
68. Sun, Q.; Luo, T.; Ren, Y.; Florey, O.; Shirasawa, S.; Sasazuki, T.; Robinson, D.N.; Overholtzer, M. Competition between human cells by entosis. *Cell Res.* **2014**, *24*, 1299–1310. [\[CrossRef\]](#)
69. Fais, S. Cannibalism: A way to feed on metastatic tumors. *Cancer Lett.* **2007**, *258*, 155–164. [\[CrossRef\]](#) [\[PubMed\]](#)
70. Sharma, N.; Dey, P. Cell cannibalism and cancer. *Diagn. Cytopathol.* **2011**, *39*, 229–233. [\[CrossRef\]](#) [\[PubMed\]](#)
71. Jain, M. An overview on “cellular cannibalism” with special reference to oral squamous cell carcinoma. *Exp. Oncol.* **2015**, *37*, 242–245. [\[CrossRef\]](#)
72. Fan, J.; Fang, Q.; Yang, Y.; Cui, M.; Zhao, M.; Qi, J.; Luo, R.; Du, W.; Liu, S.; Sun, Q. Role of Heterotypic Neutrophil-in-Tumor Structure in the Prognosis of Patients with Buccal Mucosa Squamous Cell Carcinoma. *Front. Oncol.* **2020**, *10*, 541878. [\[CrossRef\]](#) [\[PubMed\]](#)
73. Wheatley, D.N. Cellular engulfment of erythrocytes. *Br. J. Exp. Pathol.* **1968**, *49*, 541–543.
74. Chemnitz, J.; Bichel, P. Tumour cell-tumour cell emperipolesis studied by transmission electron microscopy. *Exp. Cell Res.* **1973**, *82*, 319–324. [\[CrossRef\]](#)
75. Baumgart, T.; Hess, S.T.; Webb, W.W. Imaging coexisting fluid domains in biomembrane models coupling curvature and line tension. *Nature* **2003**, *425*, 821–824. [\[CrossRef\]](#) [\[PubMed\]](#)
76. Betzig, E.; Patterson, G.H.; Sougrat, R.; Lindwasser, O.W.; Olenych, S.; Bonifacino, J.S.; Davidson, M.W.; Lippincott-Schwartz, J.; Hess, H.F. Imaging intracellular fluorescent proteins at nanometer resolution. *Science* **2006**, *313*, 1642–1645. [\[CrossRef\]](#) [\[PubMed\]](#)
77. Mary, G.; Malgras, B.; Perez, J.E.; Nagle, I.; Luciani, N.; Pimpie, C.; Asnacios, A.; Pocard, M.; Reffay, M.; Wilhelm, C. Magnetic Compression of Tumor Spheroids Increases Cell Proliferation In Vitro and Cancer Progression In Vivo. *Cancers* **2022**, *14*, 366. [\[CrossRef\]](#) [\[PubMed\]](#)
78. Leonard, F.; Godin, B. 3D in vitro model for breast cancer research using magnetic levitation and bioprinting method. *Methods Mol. Biol.* **2016**, *1406*, 239. [\[CrossRef\]](#)
79. Menegakis, A.; Klompmaker, R.; Vennin, C.; Arbusà, A.; Damen, M.; van den Broek, B.; Zips, D.; van Rheeën, J.; Krenning, L.; Medema, R.H. Resistance of Hypoxic Cells to Ionizing Radiation Is Mediated in Part via Hypoxia-Induced Quiescence. *Cells* **2021**, *10*, 610. [\[CrossRef\]](#)
80. Natânia de Souza-Araújo, C.; Rodrigues Tonetti, C.; Cardoso, M.R.; Lucci de Angelo Andrade, L.A.; Fernandes da Silva, R.; Romani Fernandes, L.G.; Guimarães, F. Three-Dimensional Cell Culture Based on Magnetic Fields to Assemble Low-Grade Ovarian Carcinoma Cell Aggregates Containing Lymphocytes. *Cells* **2020**, *9*, 635. [\[CrossRef\]](#)
81. Pandey, M.; Singh, S.; Yadav, M.; Singh, D.; Onteru, S.K. Transcriptome analysis of buffalo granulosa cells in three dimensional culture systems. *Mol. Reprod. Dev.* **2021**, *88*, 287–301. [\[CrossRef\]](#)
82. Sun, W.; Luo, Z.; Lee, J.; Kim, H.J.; Lee, K.J.; Tebon, P.; Feng, Y.; Dokmeci, M.R.; Sengupta, S.; Khademhosseini, A. Organ-on-a-Chip for Cancer and Immune Organs Modeling. *Adv. Healthc. Mater.* **2019**, *8*, 1801363. [\[CrossRef\]](#)
83. Bajpai, P.; Banerjee, N.S.; Moore, D.W.; Kim, H.G.; Afaq, F.; Contreras, C.M.; Heslin, M.J.; Reddy, V.B.; Peter, S.; Varambally, S.; et al. Developing 3D Organoid Raft Cultures from Patient-Derived Xenografts as Rapid Models to Screen Efficacy of Experimental Therapeutics. *Int. J. Mol. Sci.* **2022**, *23*, 14392. [\[CrossRef\]](#)
84. Leenhardt, R.; Camus, M.; Mestas, J.L.; Jeljeli, M.; Abou Ali, E.; Chouzenoux, S.; Bordacahar, B.; Nicco, C.; Batteux, F.; Lafon, C.; et al. Ultrasound-induced Cavitation enhances the efficacy of Chemotherapy in a 3D Model of Pancreatic Ductal Adenocarcinoma with its microenvironment. *Sci. Rep.* **2019**, *9*, 18916. [\[CrossRef\]](#)
85. Noel, P.; Muñoz, R.; Rogers, G.W.; Neilson, A.; Von Hoff, D.D.; Han, H. Preparation and Metabolic Assay of 3-dimensional Spheroid Co-cultures of Pancreatic Cancer Cells and Fibroblasts. *J. Vis. Exp.* **2017**, *2017*, e56081. [\[CrossRef\]](#)
86. Baillargeon, P.; Shumate, J.; Hou, S.; Fernandez-Vega, V.; Marques, N.; Souza, G.; Seldin, J.; Spicer, T.P.; Scampavia, L. Automating a Magnetic 3D Spheroid Model Technology for High-Throughput Screening. *SLAS Technol.* **2019**, *24*, 420–428. [\[CrossRef\]](#) [\[PubMed\]](#)
87. Xu, R.; Zhou, X.; Wang, S.; Trinkle, C. Tumor organoid models in precision medicine and investigating cancer-stromal interactions. *Pharmacol. Ther.* **2021**, *218*, 107668. [\[CrossRef\]](#)

88. Chitturi Suryaprakash, R.T.; Kujan, O.; Shearston, K.; Farah, C.S. Three-Dimensional Cell Culture Models to Investigate Oral Carcinogenesis: A Scoping Review. *Int. J. Mol. Sci.* **2020**, *21*, 9520. [[CrossRef](#)] [[PubMed](#)]
89. Santi, A.; Kugeratski, F.G.; Zanivan, S. Cancer Associated Fibroblasts: The Architects of Stroma Remodeling. *Proteomics* **2018**, *18*, 1700167. [[CrossRef](#)] [[PubMed](#)]
90. Ham, S.L.; Thakuri, S.; Plaster, M.; Li, J.; Luker, K.E.; Luker, G.D.; Tavana, H. Three-dimensional tumor model mimics stromal-breast cancer cells signaling. *Oncotarget* **2018**, *9*, 249. [[CrossRef](#)] [[PubMed](#)]
91. Overholtzer, M.; Mailleux, A.A.; Mouneimne, G.; Normand, G.; Schnitt, S.J.; King, R.W.; Cibas, E.S.; Brugge, J.S. A Nonapoptotic Cell Death Process, Entosis, that Occurs by Cell-in-Cell Invasion. *Cell* **2007**, *131*, 966–979. [[CrossRef](#)] [[PubMed](#)]
92. Balvan, J.; Gumulec, J.; Raudenska, M.; Krizova, A.; Stepka, P.; Babula, P.; Kizek, R.; Adam, V.; Masarik, M. Oxidative Stress Resistance in Metastatic Prostate Cancer: Renewal by Self-Eating. *PLoS ONE* **2015**, *10*, e0145016. [[CrossRef](#)]
93. Tahmasebi, E.; Alikhani, M.; Yazdani, A.; Yazdani, M.; Tebyanian, H.; Seifalian, A. The current markers of cancer stem cell in oral cancers. *Life Sci.* **2020**, *249*, 117483. [[CrossRef](#)]
94. Dourado, M.R.; Korvala, J.; Åström, P.; De Oliveira, C.E.; Cervigne, N.K.; Mofatto, L.S.; Bastos, D.C.; Messetti, A.C.P.; Graner, E.; Leme, A.F.P.; et al. Extracellular vesicles derived from cancer-associated fibroblasts induce the migration and invasion of oral squamous cell carcinoma. *J. Extracell. Vesicles* **2019**, *8*, 1578525. [[CrossRef](#)]
95. Kato, K.; Miyazawa, H.; Kawashiri, S.; Lambert, D.W. Tumour: Fibroblast Interactions Promote Invadopodia-Mediated Migration and Invasion in Oral Squamous Cell Carcinoma. *J. Oncol.* **2022**, *2022*, 5277440. [[CrossRef](#)]
96. Zhang, J.Y.; Zhu, W.W.; Wang, M.Y.; Zhai, R.D.; Wang, Q.; Shen, W.L. Cancer-associated fibroblasts promote oral squamous cell carcinoma progression through LOX-mediated matrix stiffness. *J. Transl. Med.* **2021**, *19*, 513. [[CrossRef](#)] [[PubMed](#)]
97. Tan, M.L.; Parkinson, E.K.; Yap, L.F.; Paterson, I.C. Autophagy is deregulated in cancer-associated fibroblasts from oral cancer and is stimulated during the induction of fibroblast senescence by TGF- β 1. *Sci. Rep.* **2021**, *11*, 584. [[CrossRef](#)] [[PubMed](#)]
98. Nicolas, A.M.; Pesic, M.; Engel, E.; Ziegler, P.K.; Diefenhardt, M.; Kennel, K.B.; Buettner, F.; Conche, C.; Petrocelli, V.; Elwakeel, E.; et al. Inflammatory fibroblasts mediate resistance to neoadjuvant therapy in rectal cancer. *Cancer Cell* **2022**, *40*, 168–184.e13. [[CrossRef](#)]
99. Dunning, S.; ur Rehman, A.; Tiebosch, M.H.; Hannivoort, R.A.; Haijter, F.W.; Woudenberg, J.; Heuvel, F.A.v.D.; Buist-Homan, M.; Faber, K.N.; Moshage, H. Glutathione and antioxidant enzymes serve complementary roles in protecting activated hepatic stellate cells against hydrogen peroxide-induced cell death. *Biochim. Biophys. Acta (BBA)-Mol. Basis Dis.* **2013**, *1832*, 2027–2034. [[CrossRef](#)] [[PubMed](#)]
100. Desgrosellier, J.S.; Cheresh, D.A. Integrins in cancer: Biological implications and therapeutic opportunities. *Nat. Rev. Cancer* **2010**, *10*, 9. [[CrossRef](#)] [[PubMed](#)]
101. Dini, S.; Binder, B.J.; Fischer, S.C.; Mattheyer, C.; Schmitz, A.; Stelzer, E.H.K.; Bean, N.G.; Green, J.E.F. Identifying the necrotic zone boundary in tumour spheroids with pair-correlation functions. *J. R. Soc. Interface* **2016**, *13*, 20160649. [[CrossRef](#)]
102. Sutherland, R.M. Cell and environment interactions in tumor microregions: The multicell spheroid model. *Science* **1988**, *240*, 177–184. [[CrossRef](#)]
103. Lao, Z.; Kelly, C.J.; Yang, X.-Y.; Jenkins, W.T.; Toorens, E.; Ganguly, T.; Evans, S.M.; Koch, C.J. Improved Methods to Generate Spheroid Cultures from Tumor Cells, Tumor Cells & Fibroblasts or Tumor-Fragments: Microenvironment, Microvesicles and MiRNA. *PLoS ONE* **2015**, *10*, e0133895. [[CrossRef](#)]
104. Park, J.; Lee, J.; Kwon, J.-L.; Park, H.-B.; Lee, S.-Y.; Kim, J.-Y.; Sung, J.; Kim, J.M.; Song, K.S.; Kim, K.-H. Scaffold-Free Coculture Spheroids of Human Colonic Adenocarcinoma Cells and Normal Colonic Fibroblasts Promote Tumorigenicity in Nude Mice. *Transl. Oncol.* **2016**, *9*, 79–88. [[CrossRef](#)]
105. Al Tameemi, W.; Dale, T.P.; Al-Jumaily, R.M.K.; Forsyth, N.R. Hypoxia-Modified Cancer Cell Metabolism. *Front. Cell Dev. Biol.* **2019**, *7*, 4. [[CrossRef](#)]
106. Paredes, F.; Williams, H.C.; San Martin, A. Metabolic adaptation in hypoxia and cancer. *Cancer Lett.* **2021**, *502*, 133. [[CrossRef](#)] [[PubMed](#)]
107. Schwegler, M.; Wirsing, A.M.; Schenker, H.M.; Ott, L.; Ries, J.M.; Büttner-Herold, M.; Fietkau, R.; Putz, F.; Distel, L.V. Prognostic Value of Homotypic Cell Internalization by Nonprofessional Phagocytic Cancer Cells. *Biomed Res. Int.* **2015**, *2015*, 359392. [[CrossRef](#)] [[PubMed](#)]

Disclaimer/Publisher's Note: The statements, opinions and data contained in all publications are solely those of the individual author(s) and contributor(s) and not of MDPI and/or the editor(s). MDPI and/or the editor(s) disclaim responsibility for any injury to people or property resulting from any ideas, methods, instructions or products referred to in the content.